Effect of Shielding Gas Oxygen Activity on Weld Metal Microstructure of GMA Welded Microalloyed HSLA Steel

Shielding gas composition is shown to have a significant influence on the formation of desirable microstructures

BY R. E. FRANCIS, J. E. JONES AND D. L. OLSON

ABSTRACT. The nucleation and growth phenomena that characterize the transformation of austenite in the weld metal of microalloyed HSLA steels are influenced by both cooling rate and composition. An important part of the compositional influence is the oxide particle nucleants that form during the welding process. The compositions of welding wire and shielding gas in GMA welds of microalloyed HSLA steels determine the oxide particle formation; consequently, the welding wire and shielding gas combination is more important than the choice of either wire or gas alone. In this investigation, the wire composition, oxygen activity of the shielding gas, and heat input were varied to study the effects of each. Several mixtures of argon plus oxygen or argon plus carbon dioxide were used.

Introduction

In recent years, there has been an increase in the use of both automatic and semiautomatic gas metal arc (GMA) welding of microalloyed high-strength low-alloy (HSLA) steels. Microalloyed HSLA steels typically exhibit a combination of moderately high yield strength and good low-temperature fracture toughness. By the use of appropriate thermal-mechanical processing, the material properties are developed in the base metal prior to the welding process. However, many of the applications for these materials require fabrication. Consequently, welding consumables must be designed and used so that the combination of toughness and high yield strength will develop in the as-solidified weld metal.

Since the weld metal mechanical properties are dependent on the microstructure, changes in the heating and cooling rates and the weld metal composition will affect the mechanical properties of the weld metal (Refs. 1-5). Two primary changes occur in the weld metal microstructure due to alteration of the cooling rate. First, a decreased cooling rate will produce generally coarser microstructural features. Second, changes in cooling rate will influence the nucleation and growth processes involved in the decomposition of austenite into ferrite plus carbides or martensite. In the case of a single weld pass, any prior thermal-mechanical history is obliterated by the melting process; consequently, the solidification microstructure will depend on the composition, nucleant formation and the weld cooling rate. For the reheat zone in a multiple-pass weld, the thermal experience of subsequent beads must also be considered.

The microstructures of microalloyed HSLA steel weld metal can be characterized into four general categories as seen in Figs. 1A-E. Blocky or grain boundary ferrite, often accompanied by Widmanstätten-type side plates, will form if the cooling rate is sufficiently slow. At a somewhat faster cooling rate, and if appropriate nucleants are available and sufficiently well distributed, a fine structure known as acicular ferrite can form. The acicular ferrite is the most favorable microstructure with respect to mechanical properties, particularly fracture toughness. Even faster cooling rates generally result in a bainitic structure, also known as aligned carbides plus ferrite. With greater cooling rates, it is possible for the austenite to transform to martensite.

An important welding parameter that can influence the mechanical properties of the GMA HSLA steel weldment is the cover gas composition. Specifically, variations in the oxygen activity can cause changes in the weld metal microstructure and mechanical properties. The shielding gas oxygen activity will influence the amount, size and composition of oxide inclusions formed in the weld metal. These oxide inclusions will act as nucleation sites and promote the decomposition of austenite upon cooling (Ref. 6). This behavior is manifest as a shift to the left (decreased reaction time) of the curves in a CCT diagram as shown schematically in Fig. 2.

This investigation was designed to study the effect of variations in cooling rate (heat input) and cover gas oxygen content on the weld metal microstructure associated with microalloyed HSLA line pipe steel. In addition, two different filler metal compositions were used to examine the relative effect of changes in a hardenability agent (manganese) and a deoxidizer (silicon) on the weld metal microstructure. This investigation examines the nature and location of the gas/metal reactions to determine if they occur primarily in the weld pool or in the metal droplet.

KEYWORDS

Shielding Gas Oxygen
GMA Weld Metal
Microalloyed Steel
HSLA Steel Weld
Weld Microstructure
Oxygen Activity
Oxide Nucleants
Austenite Transformation
Gas/Metal Reactions
Chemical Composition

Experimental Procedure

A test matrix was devised that gave variations in heat input, cover gas composition and welding wire composition. The base metal was molybdenum-niobium microalloyed HSLA pipeline steel (X-70). The 0.652-in. (16-mm) thick steel plate was flame cut into welding coupons measuring 5 in. (127 mm) by 19 in. (480 mm). Each coupon was rough ground and then dry iron shot-blasted to remove all scale

R. E. FRANCIS, J. E. JONES and D. L. OLSON are with the Center for Welding Research, Colorado School of Mines, Golden, Colo.

prior to welding. The plate chemical analysis is given in Table 1.

Two welding wire compositions were used; the compositions are shown in Table 2. The welding wires were 0.062-in. (1.6-mm) diameter and were copper flashed. They had AWS designations of ER70S-3 and ER70S-6. The primary difference in the two wires was their manganese and silicon contents. It should be noted that the high oxygen content of the wires is likely due to the copper coating.

The cover gas oxygen activity was varied by additions of oxygen or carbon dioxide to argon. Oxygen was added in 1% increments between pure argon and 5% oxygen. Carbon dioxide was added to pure argon in varying amounts, as shown in Table 3. The cover gas varied from pure argon to 100% CO_2. The matrix of welds produced for each welding wire composition is shown schematically in Fig. 3. All gas flow rates during welding were held at constant 35 ft^3/min.

Three different heat inputs were used in the study: 20, 40 and 80 kJ/in. (0.8, 1.6 and 3.2 kJ/mm). This resulted in three different cooling rates so that the kinetics of the solid-state reactions could be studied. A constant-potential power supply was used, and the welding voltage was held constant at 25 V for all welds produced. A constant wire feed rate was maintained for all welds; however, a slight variation in current was observed due to changes in the composition of the cover gas. Consequently, the welding current was 280 ± 20 A. These heat input differences were corrected by changing the travel speed of the welding gun. All welds were made using direct current electrode-positive (DCEP) power.

For this investigation, only fully automatic GMA bead-on-plate welds were used. Following the welding process, each weld was sectioned, macroetched and photographed in order to make dilution measurements. The metallic composition of welding wire, base plate and weld deposits were made using a computer-controlled Bausch and Lomb emission spectrograph. A Leco interstitial analyzer was used to determine weld metal carbon, oxygen and nitrogen contents.

Finally, weld metal metallographic specimens were removed from each weldment and examined. Photomicrography was used to produce representative microstructural evidence from each weld. Each representative microstructure was taken at a depth below the weld bead crown surface approximately in line with the top surface of the base plate and at the longitudinal centerline of the weld. Each weld metal microstructure observed was examined and categorized as to the predominant features.

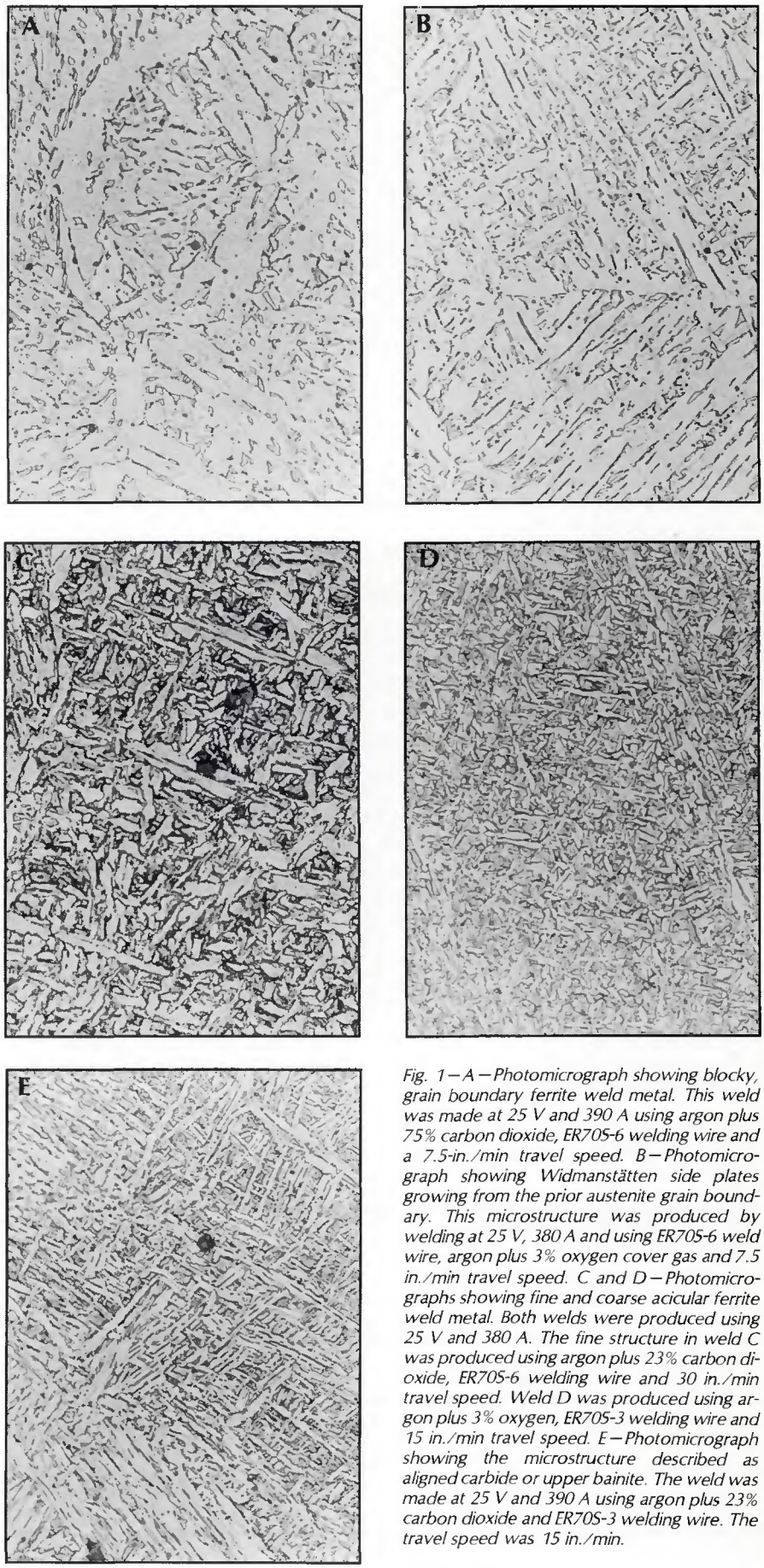

Fig. 1—A—Photomicrograph showing blocky, grain boundary ferrite weld metal. This weld was made at 25 V and 390 A using argon plus 75% carbon dioxide, ER70S-6 welding wire and a 7.5-in./min travel speed. B—Photomicrograph showing Widmanstätten side plates growing from the prior austenite grain boundary. This microstructure was produced by welding at 25 V, 380 A and using ER70S-6 weld wire, argon plus 3% oxygen cover gas and 7.5 in./min travel speed. C and D—Photomicrographs showing fine and coarse acicular ferrite weld metal. Both welds were produced using 25 V and 380 A. The fine structure in weld C was produced using argon plus 23% carbon dioxide, ER70S-6 welding wire and 30 in./min travel speed. Weld D was produced using argon plus 3% oxygen, ER70S-3 welding wire and 15 in./min travel speed. E—Photomicrograph showing the microstructure described as aligned carbide or upper bainite. The weld was made at 25 V and 390 A using argon plus 23% carbon dioxide and ER70S-3 welding wire. The travel speed was 15 in./min.

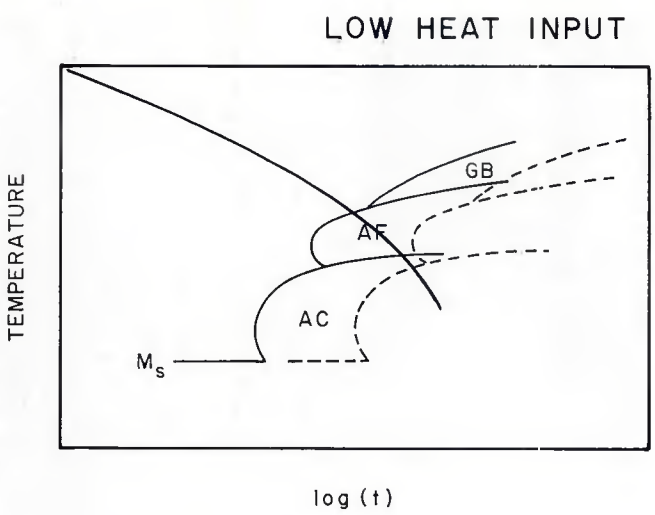

Fig. 2—Simulated temperature log-time diagram that illustrates the resultant shift to the right of the ferrite initiation curve with either a decrease in the oxide-forming propensity (O + Si/4) or an increase in the hardenability (Mn). Refer also to Fig. 11.

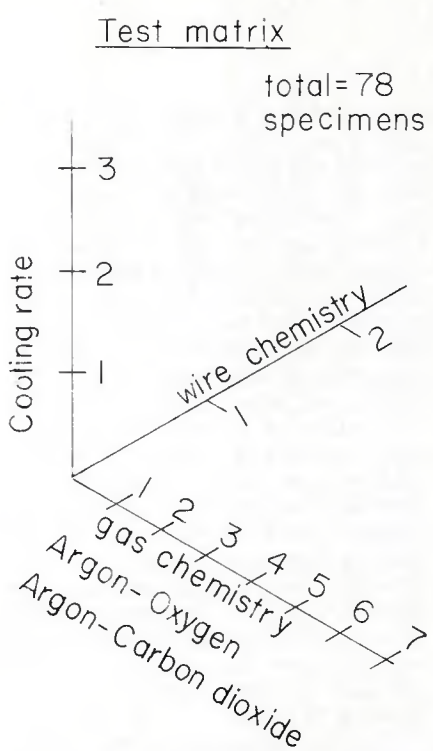

Fig. 3—Schematic diagram showing the test matrix used for this investigation. Variations were made in cooling rate, welding wire composition and shielding gas composition.

Table 1—High-Strength Low-Alloy (X-70) Line Pipe Steel Chemical Analysis (wt-%)

C	Mn	Si	Ni	Mo	Cr	P	S	Nb	Cu
0.08	1.58	0.26	0.11	0.34	0.10	0.011	0.001	0.03	0.37

Results and Discussion

Two separate studies were conducted in this investigation. First, the gas/metal reactions were studied to determine the effect of cover gas composition on the final weld metal composition. Second, the effect of changes in weld metal chemical composition on the resultant weld metal microstructure was examined.

Gas/Metal Reactions

Two parameters were calculated from the chemical analysis data. The first parameter, Δ_{ele}, is the difference between the actual weld metal chemical content for a particular constituent $[X]^{act}_{ele}$, and the back-calculated chemical composition $[X]^{calc}_{ele}$ assuming only dilution:

$$\Delta_{ele} = [X]^{act}_{ele} - [X]^{calc}_{ele} \quad (1)$$

The calculated nominal chemical content of a specific element $[X]^{calc}_{ele}$ is made using the assumption that no change in composition will take place during welding. The calculation is based on the dilution of filler metal (wire) and the melted base metal (plate) and is calculated based on the relative volume fractions of each as a premultiplier of the respective composition amounts. It is also assumed that the area fractions of a weld transverse cross-section (Fig. 4) are a good estimate of the weld volume fractions. The value of $[X]^{calc}_{ele}$ is then calculated as:

$$[X]^{calc}_{ele} = [X]^{wire}_{ele} A_{filler} + [X]^{plate}_{ele} A_{plate} \quad (2)$$

where $[X]^{wire}_{ele}$ is the elemental content of the wire, A_{filler} is the cross-sectional area fraction of the crown of the weld above the plate relative to the area of the total fusion zone area, $[X]^{plate}_{ele}$ is the elemental composition of the base plate, and A_{plate} is the cross-sectional area fraction of the fusion zone below the surface of the plate relative to the total fusion area. A positive value of Δ_{ele} would indicate that there was pickup of that particular element from some sources other than the welding wire or base plate. Those sources would be the other welding consumable, (*i.e.,* cover gas), the atmosphere (*e.g.,* nitrogen), or contamination (*e.g.,* hydrogen from a dirty base plate). A negative value of "delta" would indicate loss of the element during welding due to such occurrences as chemical reaction with the welding cover gas, mechanical loss such as spatter, or simple volatization of that element in the arc.

The second parameter calculated is the droplet composition ($[X]^{trans}_{ele}$) at the time it entered the weld pool, assuming all of the gas metal reactions take place in the droplet and no changes to the composition occur due to reactions of the cover gas with the liquid weld pool. This material transfer (droplet composition) parameter, $[X]^{trans}_{ele}$, is calculated by the equation:

$$[X]^{trans}_{ele} = \frac{[X]_{weld} - A_{plate}[X]^{plate}_{ele}}{A_{filler}} \quad (3)$$

Figures 5 and 6 are diagrams showing, 1) the actual measured weld metal oxygen; 2) the calculated Δ_{ele} values for oxygen; and 3) the material transfer parameter for oxygen as a function of percent oxygen or percent carbon dioxide in the cover gas. The results for both ER70S-3 and ER70S-6 are shown. These data rep-

Table 2—Welding Wire Chemical Analysis (wt-%)

C	Mn	Si	Ni	Mo	Cr	Nb	Cu	O	Class
0.13	1.19	0.61	0.015	0.01	0.06	0.003	0.05	0.022	ER70S-3
0.11	1.60	1.02	0.040	0.01	0.08	0.003	0.14	0.014	ER70S-6

Wire diameter: 0.0625 in.

Table 3—Composition of Shielding Gases: wt-% Oxygen or Carbon Dioxide in Argon

Gas	Percentage in Argon							
Oxygen	0	0.92	2.28	3.25	4.06	5.22	—	—
Carbon Dioxide	0	10.3	14.4	23.1	28.5	52.3	75.4	99.2

The flow rate was held at a constant 35 cfh.

resent approximately 140 data points for each graph. The three heat input differences resulted in sufficiently different cooling rates so that the reactions that alter chemical compositions were significantly influenced. The degree to which those reactions proceeded resulted in differences in the composition of the cooled weld deposit. Consequently, bands (labeled "−3" and "−6") rather than lines are shown on the figures to indicate the trends observed. In addition, the effect of heat input is also shown, thus indicating the direction of approach of thermodynamic equilibrium.

The oxygen activity as influenced by the oxygen or carbon dioxide content of the cover gas has an influence on the weld metal oxygen content. In each case, increasing the oxygen activity of the shielding gas increased the weld metal oxygen content. The influence of the atmosphere is also evident in that as the heat input increased, the oxygen content increased within each band. Since the heat input varied only by a change in travel speed, an increase in heat input represents a longer time to solidify and thus a longer time of exposure of the weld pool to the atmosphere after the welding gun and cover gas envelope have passed. Similar conclusions were found by Grong and Christensen (Ref. 11) and by Coe and Moreton (Ref. 12).

The oxygen transfer parameter is assumed to represent the oxygen content of the droplets as they arrive in the molten pool, assuming that no further reactions with oxygen in the cover gas take place in the weld pool. However, in both cases (oxygen or carbon dioxide additions), the oxygen transfer parameter is negative for low-oxygen-potential cover gas. It is physically impossible for the oxygen content of the droplets to be negative. Consequently, it must be concluded that gas/metal reactions in the weld pool represent a significant contribution to the total gas/metal reaction. Thus, despite the larger surface area-to-volume ratio of the metal droplets causing the droplets to be the classic model primary gas/metal reaction site, the present data indicate that much of the reaction takes place instead in the weld pool. The same trends have been found by Grong and Christensen (Ref. 11). Work by Coe and Moreton (Ref. 12) on equilibrium between carbon and oxygen in the weld shows a best fit of their data is the temperature range just before freezing. In other words, there is adequate time before solidification for the dissolved gases and weld pool to reach near-equilibrium.

Oxygen is only slightly soluble in iron. Consequently, most of the oxygen content of the weld metal is in the form of oxides. Figures 7 and 8 illustrate the effect of cover gas oxygen activity on the weld metal manganese content. Again, these figures are divided into three parts: 1) the

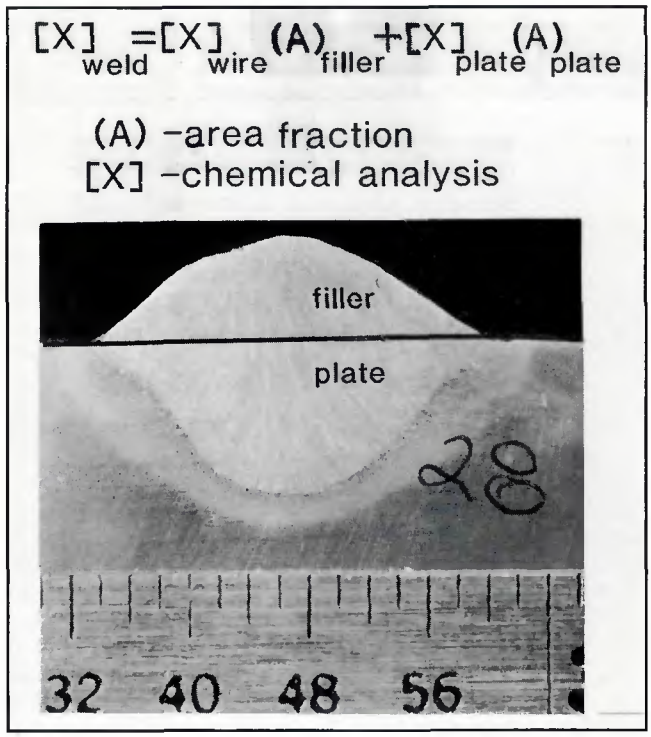

Fig. 4—Illustration of computation of the back-calculated chemistry of the weld deposit assuming only dilution.

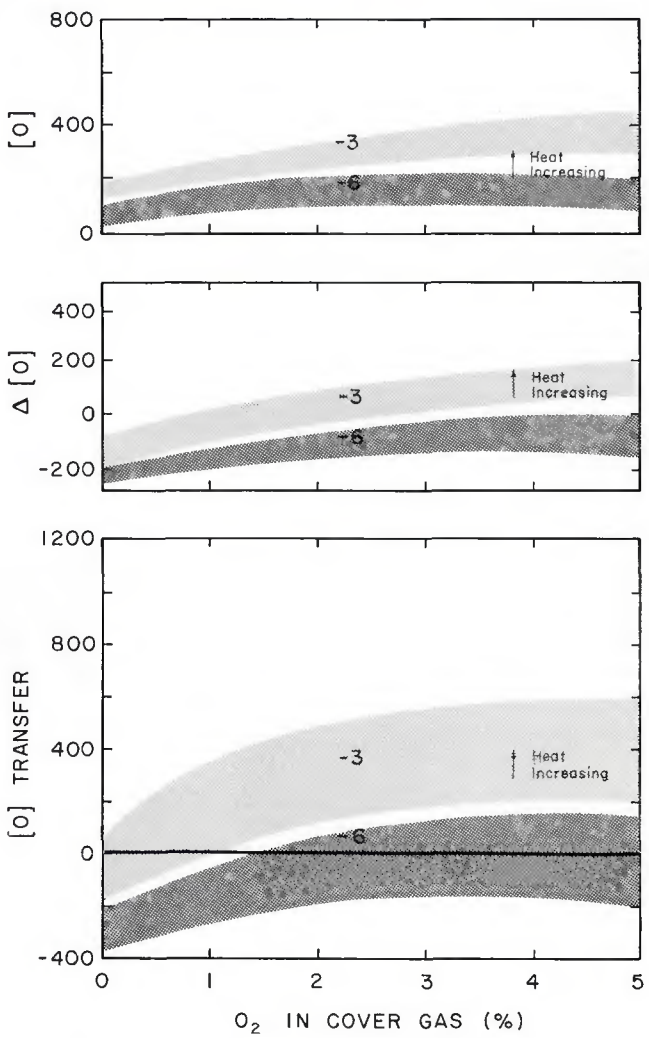

Fig. 5—Plots of data bands for oxygen in welds as a function of the percentage oxygen in the cover gas. [O] is the analyzed weight parts per million of oxygen, Δ [O] is the delta oxygen, and [O] TRANSFER is the calculated composition transferred. Note: the identifiers −3 and −6 refer to welds produced with ER70S-3 and ER70S-6 welding wires, respectively.

actual weld metal manganese content; 2) the calculated delta manganese; and 3) the manganese transfer parameter.

The two welding wires ER70S-3 and ER70S-6 had different amounts of manganese. Consequently, the metal droplets transferred and the weld pools resulting from each wire had different manganese activity levels. However, the delta plot for manganese indicates that the reaction rate was essentially identical for each wire composition since only one band of data appears. This indicates that the reaction involving manganese and oxygen was limited by the kinetics and not by the manganese activity in the metal.

Although a percentage of the manganese is lost through the formation of oxides that float to the surface of the melt and further is lost due to its high vapor pressure, some of the manganese is tied up in the form of oxides dispersed within the solidified weld pool. These finely distributed oxides contribute to the transformation kinetics of the solidified metal as it cools to room temperature following welding.

Microstructure-Composition Effects

The second phase of investigation was a study of the weld metal microstructure as a function of its composition. The microstructure depends primarily on the cooling rate and chemical composition. The cooling rate is a direct function of the heat input, plate thickness, the preheat, the postweld heat treatment and the indirect function of voltage, current, travel speed and heat transfer efficiency. The weld metal composition is a function of the composition of the cover gas, welding wire, base metal and time allowed for reaction. Examining a schematic temperature log-time diagram (Fig. 2), it becomes evident that a slow cooling rate will produce blocky ferrite or grain boundary ferrite. A faster cooling rate can pass into a fairly narrow window of acicular ferrite. An even faster cooling rate passes through the aligned ferrite or bainite region.

Kikuta, *et al.* (Ref. 13), found that if the notch toughness of electroslag welds was plotted as a function of oxygen content and manganese content, an island of very good notch toughness occurred. This was associated with acicular ferrite when they examined the microstructure. The notch toughness was found to decrease with changes in oxygen and manganese contents. The microstructure coarsened as oxygen increased and manganese decreased, and progressed to aligned carbides as oxygen decreased and manganese increased. The acicular ferrite with its fine microstructure and random orientation is a relatively tough material. The basket-weave structure resists propagation of the fracture. The blocky and grain boundary ferrite have long, straight fracture paths available, as is also the case with the needles of the bainite with their high

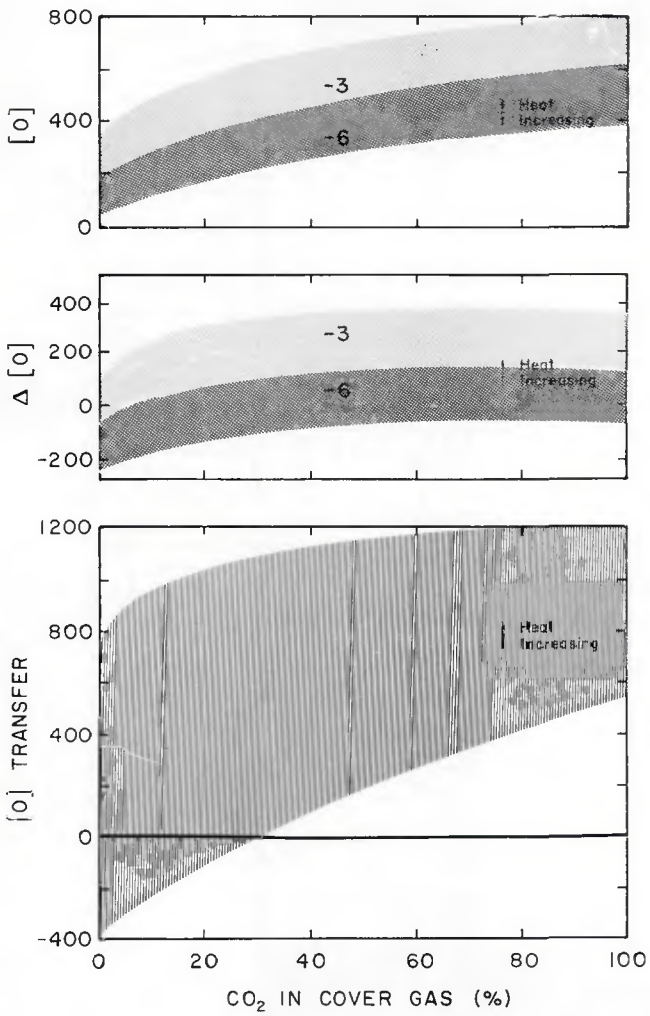

Fig. 6 — Plots of data bands for oxygen in welds as a function of the percentage carbon dioxide in the cover gas. [O] is the analyzed weight parts per million of oxygen, Δ [O] is the delta oxygen, and [O] TRANSFER is calculated composition transferred. Note: the identifiers −3 and −6 refer to welds produced with ER70S-3 and ER70S-6 wires, respectively.

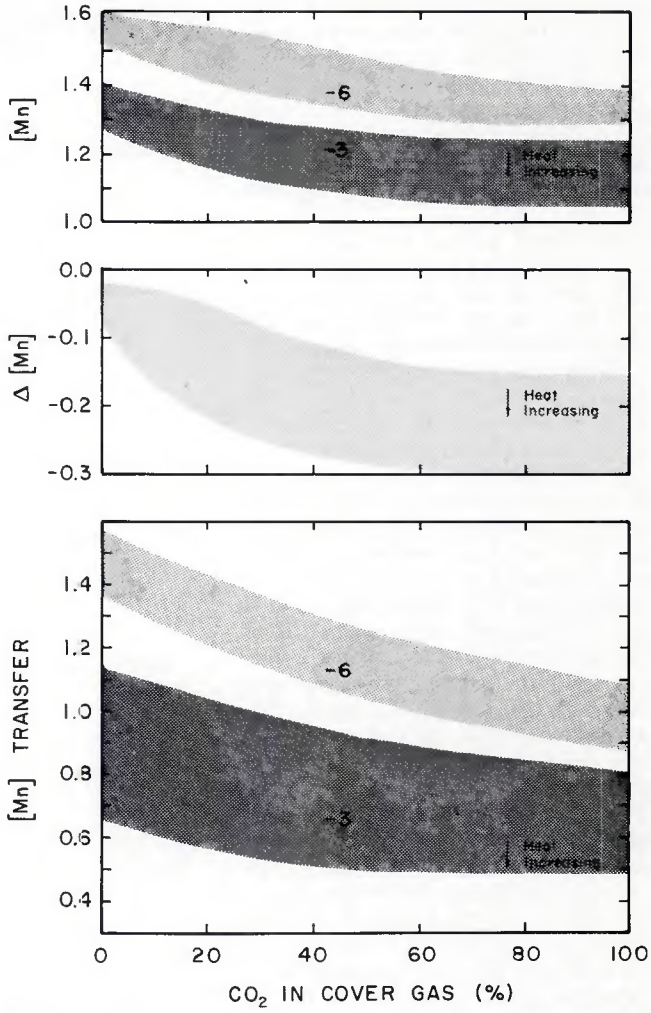

Fig. 7 — Plots of data bands for wt-% manganese as a function of the percentage carbon dioxide in the cover gas. [Mn] is the analyzed wt-% of manganese in the weld; Δ [Mn] is the delta manganese, and [Mn] TRANSFER is the calculated composition transferred. Note: the identifiers −3 and −6 refer to welds made with ER70S-3 and ER70S-6 wires, respectively.

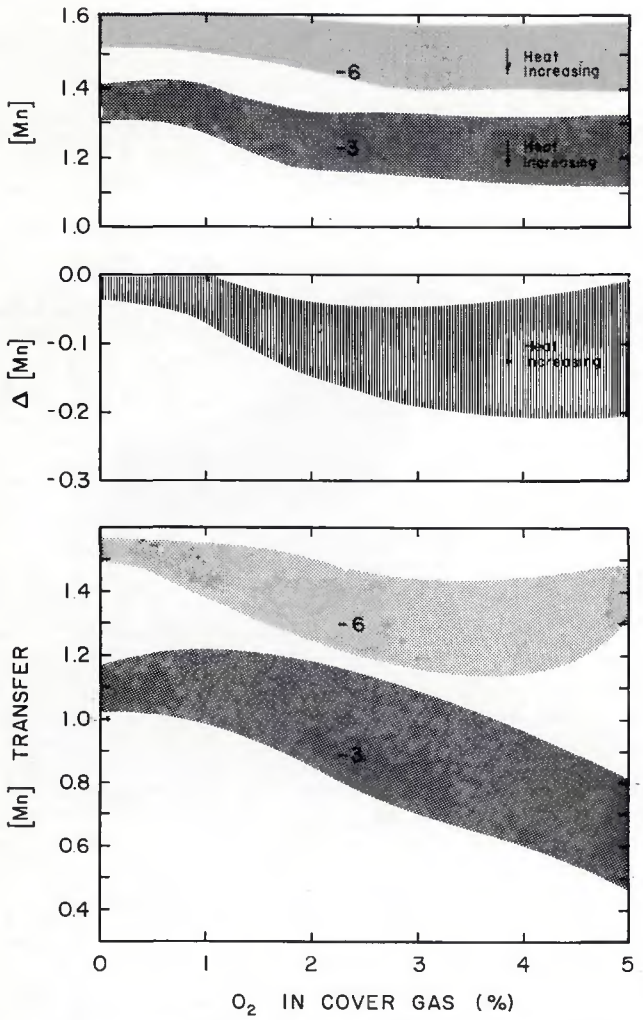

Fig. 8—Plots of data bands for wt-%manganese as a function of the percentage oxygen in the cover gas. [Mn] is the analyzed wt-% of manganese in the weld; Δ [Mn] is the delta manganese and [Mn] TRANSFER is the calculated composition transferred. Note: the identifiers −3 and −6 refer to welds made with ER70S-3 and ER70S-6 wires, respectively.

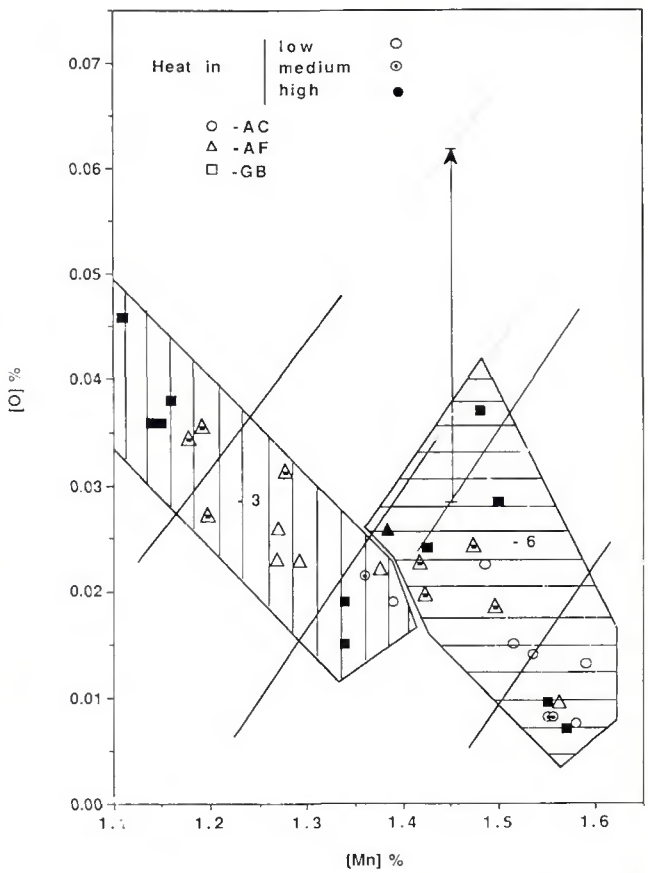

Fig. 9—Diagram of the derived weld microstructure as a function of the weld oxygen and manganese compositions. Data for the welds made with ER70S-3 welding wire are toward the left, and welds made with ER70S-6 are toward the right.

aspect ratio. Other work by Dallam, *et al.* (Ref. 1), showed similar results with submerged arc welds.

By plotting the microstructure results obtained in this study using the GMA welding process with argon-oxygen cover gas, a diagram similar to that of Kikuta, *et al.* (Ref. 13), is produced. However, the two chemical compositions from the two wires map separately as seen in Fig. 9. Each wire composition gives a band of coarse microstructure at the upper left, a center band of fine acicular ferrite, and another band of aligned carbide at the lower right, having the ER70S-3 welding wire toward the left and the ER70S-6 welding wire toward the right side of the diagram.

Finely dispersed particles can affect the ferrite nucleation rate (Refs. 9,14). Since the oxide formation will be influenced both by the silicon as well as the oxygen content (Refs. 12,15), a second parameter was introduced by adding to the oxygen content one-fourth of the silicon content (corresponding to the approximate proportion of silicon in certain spinel-type oxides). This new parameter is a measure of the oxide-forming propensity of the weld metal, while the manganese content represents the hardenability agent available.

The plot of microstructure as a function of this new parameter and percent manganese is shown in Fig. 10. The data now convert into a unified map and represent microstructure as a function of hardening agents (manganese) on the horizontal axis and dispersed oxide particles on the vertical axis. The results illustrated in Fig. 10 can be related to the CCT diagram. For a particular cooling rate that crosses into the grain boundary ferrite region, changes in composition, which result in an increase in the manganese or a decrease in the oxide content, will shift the initiation curve as illustrated in Fig. 11. This can result in the formation of an acicular ferrite. Likewise, an acceptable microstructure from a particular cooling curve can be lost by shifting out of that acceptable (acicular ferrite) region by either increasing the manganese or decreasing the oxide content into the aligned ferrite or bainite region.

As a matter of practical interest there is only a limited number of parameters under the control of the welding engineer. Figures 12 and 13 show the regions of preferred microstructure as a function of heat input and cover gas composition for each of the welding wires used. It is apparent that each wire has an optimum region. Thus, it is important that the choice of welding wire for a particular application be coupled with the choice of shielding gas. For example, it can be seen from this work that with the argon-oxygen cover gas, a greater range in heat input can give acceptable welds between 2–4% oxygen in argon with either welding wire, and the use of an argon-carbon dioxide cover gas will restrict both the heat input and the choice of wire composition.

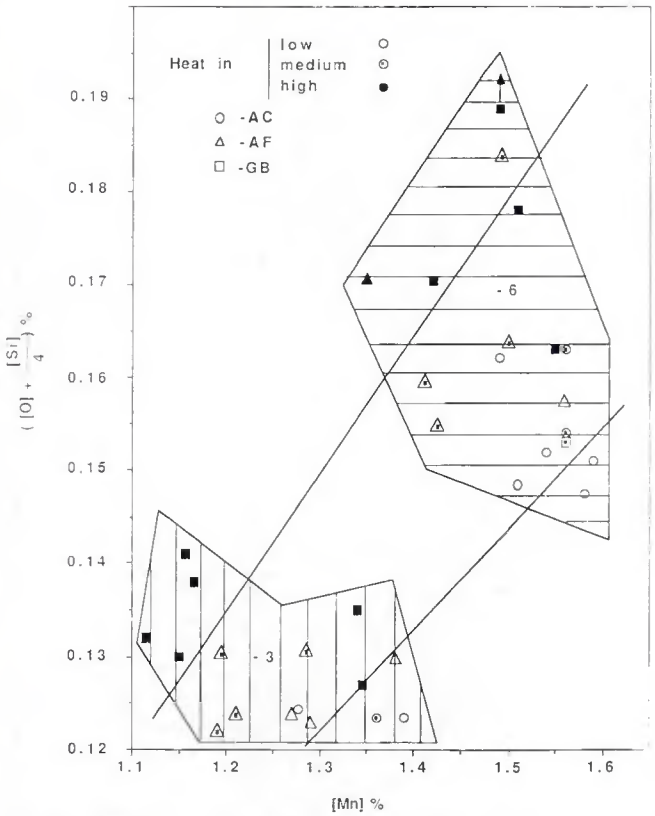

Fig. 10—Diagram of the derived weld microstructure as a function of the oxide-forming propensity (O + [Si]/4) and the hardenability (manganese).

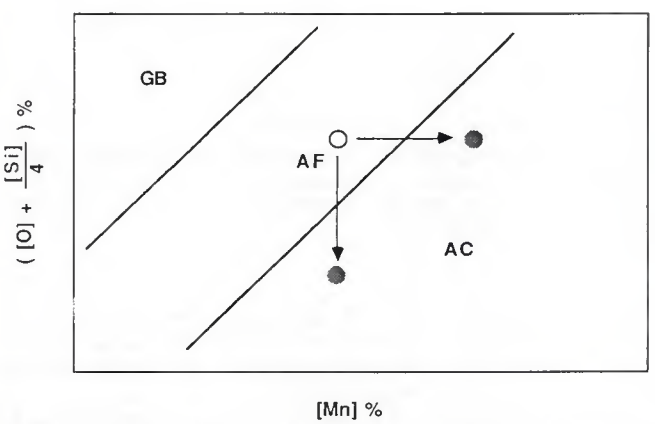

Fig. 11—Showing a plot of oxide-forming propensity vs. hardenability. Notice that either an increase in hardenability or a decrease in oxide-forming propensity will shift from an acceptable microstructure to one of aligned carbide.

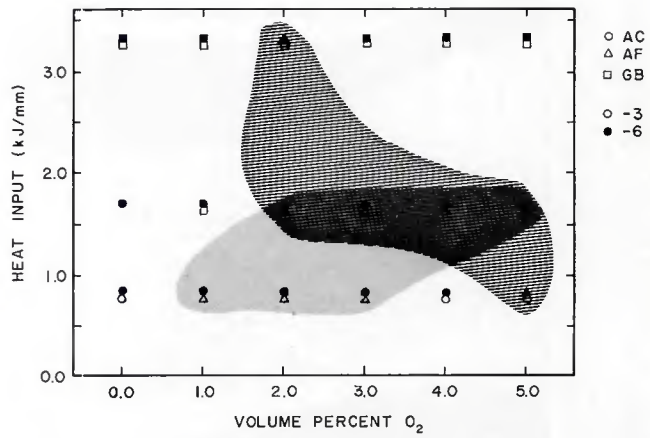

Fig. 12—Map of microstructure as a function of heat input, cover gas and welding wire type. The shaded area delineates the areas of acicular ferrite. The lined area silhouettes the ER70S-6 produced welds, and the dotted area the ER70S-3 produced welds. The cover gas was argon plus oxygen.

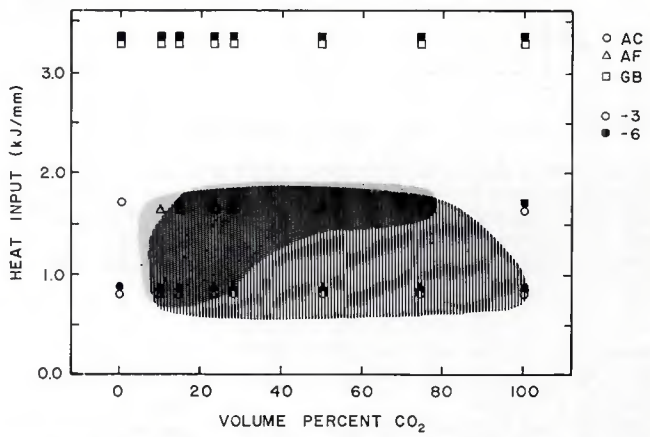

Fig. 13—Map of microstructure as a function of heat input, cover gas and welding wire type. The shaded area delineates the areas of acicular ferrite. The lined area silhouettes the ER70S-6 produced welds, and the dotted area the ER70S-3 produced welds. The cover gas was argon plus carbon dioxide.

Conclusions

1) The volume fraction of acicular ferrite is definitely influenced by the oxygen and carbon dioxide content in the argon cover gas.

2) Plots of inclusion-forming agent vs. hardenability agent can be used to predict microstructure of GMA weld metal.

3) Gas metal arc welding can achieve acceptable weld metal microstructures in niobium microalloyed steels only with the proper combination of welding wire, shielding gas and heat input.

Acknowledgment

The authors acknowledge and appreciate the research support of the United States Army Research Office.

References

1. Dallam, C. B., Liu, S., and Olson, D. L. 1985. The influence of CaO-CaF_2-SiO_2 welding flux system on the welding of niobium microalloyed HSLA steel. *Welding Journal* 64(5): 140-s to 151-s.

2. Levine, E., and Hill, D. C. 1976. Structure and properties of HSLA weld metal containing Cb or V. *Proceedings of International Conference on Welding of HSLA (Microalloyed) Structural Steels.* ASM International, p. 402.

3. Pollard, P., and Milner, D. R. 1971. Gas-metal reactions in CO_2 arc welding. *J. Steel and Iron Inst.*, pp. 291–300.

4. Abson, D. A., and Dolby, R. E. 1980. A scheme for the quantitative description of ferritic weld metal microstructure. *The Welding Institute Research Bulletin,* April, p. 100.

5. Dolby, R. E. 1976. The effect of niobium on the HAZ toughness of high heat input welds in C-Mn steels. *Proceedings from ASM Conference Welding of HSLA [Microalloyed] Structural Steels,* Rome, Italy, pp. 212–234.

6. Liu, S., and Olson, D. L. 1986. The role of inclusions in controlling HSLA steel weld metal microstructures. *Welding Journal* 65(6): 139-s to 149-s.

7. Cochrane, R. C., and Kirkwood, P. R. 1978. The effect of oxygen on weld metal microstructure. *International Conference on Trends in Steel and Consumables for Welding,* Paper 35, Welding Institute, London.

8. Harrison, P. L., and Farrar, R. A. 1981. Influence of oxygen-rich inclusions on the gamma to alpha phase transformation in high-strength low-alloy (HSLA) steel weld metals. *J. Mat. Sci.* 16, pp. 2218-2226.

9. Abson, D. J., Dolby, R. E., and Hart, P. M. H. 1978. The role of nonmetallic inclusions in ferrite nucleation in carbon steel weld metals. *International Conference on Trends in Steel and Consumables for Welding,* Paper 25, Welding Institute, London.

10. Kobayashi, T., and Sakai, Y. 1982. The effect of shielding gas composition on the characteristics of carbon steel weld metal. Japan Welding Engineering Society Report, IIW Doc. XII-E-32-82 and IIW Doc. XII-B-26-82.

11. Grong, O., and Christensen, N. 1982. Factors concerning weld metal chemistry. The Foundation of Scientific and Industrial Research at the Norwegian Institute of Technology, Final Report, Contract Number DASA 37-81-C-0309.

12. Coe, F. R., and Moreton, J. 1979. The chemistry of oxygen in gas-shielded welding of steel. The Welding Institute, Report 95.

13. Kikuta, Y., Araki, T., Honda, K., and Sakahira, S. 1980. The metallurgical properties of electroslag weld metal using CeF_3 addition wire. *Proceedings of International Conference on Welding Research in the 1980s,* Session B, pp. 131-136.

14. Indacochea, J. E., and Olson, D. L. 1983. Relationship of weld metal microstructure and penetration to weld metal oxygen content. *J. Materials for Energy Systems* 5(12), 139-148.

15. Kawawa, T., Okubo, M., Sasajima, Y., and Tokunaga, H. 1965. Rate of manganese and silicon complex [of steel]. Nihon Steel Tube Co., Ltd., translated from TETSU to HAGANE, 51(4):780-783.

16. Glover, A. G., McGrath, J. T., Tinkler, J., and Weatherly, G. C. 1977. The influence of cooling rate and composition on weld metal microstructure in a carbon/manganese and an HSLA steel. *Welding Journal* 56(9):267-s.